(2)

OFFICE OF NAVAL RESEARCH

Contract No. N00014-91-J-1409

Technical Report No. 138

Some Electrochemical Consequences of Potential-Induced Surface Reconstruction on Au(100): Double-Layer Nonuniformity and Electrode Kinetics

by

Antoinette Hamelin, Livia Stoicoviciu, Gregory J. Edens, Xiaoping Gao, and Michael J. Weaver

Prepared for Publication

in

Journal of Electroanalytical Chemistry

Department of Chemistry

Purdue University

West Lafayette, IN 47907-1393

April 1993

ABSTRACT

Some consequences of potential-induced surface reconstruction upon the double-layer structure and electrocatalytic properties of Au(100) in aqueous perchloric acid have been explored by means of cyclic voltammetry and differential capacitance measurements, along with in-situ scanning tunneling microscopy (STM). Initially unreconstructed [i.e. (1 × 1)] Au(100) yields capacitance-potential (C-E) profiles in dilute (1 mM) perchloric acid in the vicinity of the potential of zero charge, E_{pzc}, which are consistent with the presence of an essentially uniform distribution of electronic charge across the surface. Upon forming electrochemically induced hexagonal surface reconstruction by holding the potential below -0.2 V for periods up to ca 20 min, these C-E minima are broadened substantially. The latter observation implicates the presence of electrostatically distinct surface domains with "local" E_{pzc} values that are significantly (0.1-0.2 V) lower as well as higher than that for unreconstructed Au(100), having dimensions at least comparable to the Debye length of the diffuse layer, ca 9.5 nm, in 1 mM $HClO_4$. This finding is consistent with the real-space surface morphology as obtained by in-situ STM under these conditions, which shows the common presence of corrugated features, such as edges of reconstructed strands, in addition to domains featuring quasi-hexagonal atomic packing. The sharp potential-induced removal of the reconstruction inferred from the appearance of a voltammetric feature at 0.6 V vs SCE in perchloric acid is confirmed by STM data acquired during potential sweeps, which also shows that the 24% excess gold atoms released form arrays of metal clusters. The rates of proton electroreduction are significantly (1.3 to 1.7 fold) accelerated by Au(100) reconstruction. A qualitatively similar finding applies to carbon monoxide electrooxidation. These effects appear to be due to the involvement of gold atomic sites featuring lower coordination numbers seen to be formed upon surface reconstruction.

INTRODUCTION

It is now well established that Au(100) as well as other ordered low-index faces of gold in aqueous perchloric acid and other media undergo reconstruction spontaneously below the potential of zero charge, E_{pzc}. Persuasive evidence for this phenomenon, originally suggested on the basis of electrochemical results[1,2], has been obtained latterly from in-situ microscopic methods, specifically electroreflectance[2], second harmonic generation[3], and most directly from x-ray diffraction[4] and atomic-resolution scanning microscopy (STM)[5-7]. The last technique, in particular, has provided detailed information regarding the local real-space structure of the reconstructed Au(100) surface, and uncovered a myriad of long-range superstructures that can form under these conditions[6]. The basic (5 x 27) symmetry features an essentially hexagonal close-packed layer of gold atoms overlaid on the square-planar Au(100) substrate, yielding corrugations both across and along the unit cell arising from the significant compression (20% and 4%) of the atomic packing density along the short and long unit-cell directions, respectively[6].

In contrast to Au(110)[8] and higher-index gold faces[9], the potential-induced occurrence of the reconstruction on Au(100) in non- (or weakly-) adsorbing electrolytes such as perchloric acid is relatively slow, requiring at least 5-15 min to develop extensively when the potential is adjusted below E_{pzc}[2,6,7]. The subsequent lifting of the reconstruction occurs under these conditions at potentials above E_{pzc}. These sluggish dynamics offer interesting opportunities for examining the electrochemical consequences of reconstruction, since surfaces containing either predominantly (1 x 1) (i.e. unreconstructed) or (5 x 27) reconstructed domains can be arranged to be present at a given electrode potential for at least 1-2 min, depending on the previous potential history.

Reported here are some pertinent observations of the effects of surface

reconstruction on the double-layer structure and electrode kinetic properties of Au(100). The former aspect, as deduced from capacitance-potential behavior in the vicinity of E_{pzc}, can provide information on the degree of electronic charge nonuniformity at the surface induced by reconstruction. Some preliminary observations along these lines are contained in ref. 7. Some additional information regarding such surface structural changes as obtained by in-situ STM under voltammetric conditions is also reported here. The latter aspect primarily involves examining the kinetics of proton electroreduction, and also carbon monoxide electrooxidation. The choice of these two inner-sphere electrode reactions was prompted by our previous studies which indicate the presence of interesting dependencies of the rate parameters upon the crystallographic orientation of ordered gold surfaces in acidic perchlorate media[10-12]. Comparative capacitance- and rate-potential data are also reported here for Au(210) in order to ascertain in what fashion the variations in electrode-potential history, may also affect the behavior of reconstructed versus unreconstructed Au(100). The Au(210) surface provides a useful "reference system" in that essentially no influence of the electrode potential history is observed upon either the capacitance-potential or rate-potential behavior. This is consistent with the absence of potential-induced reconstruction on Au(210) as discerned by STM[13].

EXPERIMENTAL

Most experimental work was performed at LEI-CNRS. Details of the procedures used for the kinetics measurements are described in refs. 10 and 12. The gold single crystals were grown, cut, and polished at LEI-CNRS. The electrode surfaces were annealed immediately prior to use by heating to redness in an oxy-gas flame, cooled in ultrapure water, and transferred to the

electrochemical cell protected by a drop of water(vide infra). Contact with the electrolyte solution was made by means of the hanging meniscus method.

As for other studies of this type, it should be stressed that cleanliness of the gold-solution interface is essential for the electrochemical measurements to be meaningful. Cells and other glassware were rinsed with boiling water just before a given experiment. Solutions were prepared fresh with water purified just beforehand by a Millipore system. Sodium perchlorate (Pro Analysis Merck) was recrystallized and baked at 300°C before use; the perchloric acid was suprapure Merck. Oxygen was purged from the solutions by sparging with nitrogen. The reference electrode was a reversible hydrogen electrode connected by a bridge to the electrochemical cell containing the same electrolyte, eliminating any liquid junction potential. For convenience of the reader, however, the potentials are quoted here versus the conventional saturated calomel electrode (SCE). All measurements were performed at 25 (± 0.1)°C, controlled by means of a circulating water thermostat.

The in-situ STM measurements were performed at Purdue, largely as described elsewhere[5-9]. The microscope is a Nanoscope II (Digital Instruments) with a bipotentiostat for electrochemical STM. The STM tips were 0.01 in. tungsten wire etched electrochemically in 1 M KOH. The STM electrochemical cell consists of Teflon walls with the gold substrate forming the base. The counter electrode was gold and the reference electrode was a freshly electrooxidized gold wire.

RESULTS AND DISCUSSION

Capacitance-Potential Behavior

An important objective of this work is the utilization of differential capacitance-electrode (C-E) data obtained from either ac impedance or cyclic voltammetric measurements to explore the consequences of Au(100) surface

reconstruction upon the double-layer structure. A useful tactic for this purpose, especially when using electrolytes such as perchloric acid which exhibit only weak or negligible anion specific adsorption at small electrode charges, is the examination of C-E curves particularly in the vicinity of E_{pzc}. As is well known, the morphology of C-E curves obtained in dilute electrolytes under these conditions can provide information not only concerning the effective values of E_{pzc}, but also the extent to which the electronic charge is distributed uniformly across the metal surface[14] (vide infra).

Figure 1a shows a set of C-E curves obtained by means of ac impedance (20 Hz) measurements on Au(100) for two concentrations of aqueous perchloric acid, 30 and 1 mM, as indicated. The C-E curves were obtained during potential cycling between -0.5 V and 1.35 V at 5 mV s^{-1}. (These potential limits correspond approximately to the onset of hydrogen evolution and the formation of an oxide monolayer.) Data obtained during both the positive- and negative-going sweeps are shown, as solid and dashed traces, respectively. Two features of Figure 1a are of significance in the present context. Firstly, a C-E minimum is observed at 0 to 0.05 V vs. SCE, which becomes markedly deeper as the electrolyte concentration is diminished. As is well known, this behavior is a clear indicator that the potential minimum, E_{min}, can be identified with E_{pzc} (cf Figure 4a of ref. 15), resulting from the increasing influence of the diffuse-layer capacitance under these conditions.

Secondly, however, the shape as well as the potential of this diffuse-layer minimum is seen to be dependent on the direction of the potential sweep, the C-E well becoming broader and shifted significantly (by ca 0.05 V) to more positive potentials for positive-going scans (Figure 1a). The hysteresis is only evident for scans obtained following potential excursions to below about -0.2 V. Thus the dotted curve shown for 30 mM $HClO_4$ in Figure 1a, obtained during a positive-

going sweep returning only from −0.1V, is virtually identical to the dashed trace observed during the prior negative-going potential scan. The occurrence of C-E hysteresis for Au(100) has been noted earlier[2,7,15,16]; data along these lines originally prompted the suggestion by one of us that the Au(100) face undergoes reconstruction at negative electrode charges[1]. As noted above, confirmation of this phenomenon for Au(100) has been obtained recently by means of in-situ microscopic techniques[3-6].

Another clear electrochemical manifestation of the occurrence of such charge-induced reconstruction on Au(100) is evident from cyclic voltammograms gathered under similar conditions. A typical example, obtained in 1 mM $HClO_4$, is shown in Figure 2a. (The distorting influence of the large solution resistance in such a dilute electrolyte was removed by means of positive-feedback iR compensation.) In addition to a conventional cyclic voltammogram obtained at 50 mV s^{-1} between −0.5 and 1.3 V, showing the morphology of the oxide anodic formation and reduction, Figure 2a contains three voltammograms (displayed on an enlarged, 25-fold more sensitive, current scale) which refer to excursions to 1.3 V (solid curve 3) and also to lower positive potential limits (dashed trace 2 and dotted trace 1). In the absence of faradaic or other irreversible surface processes, the positive- and negative-going current-potential traces form effectively mirror images of each other, reflecting the true C-E behavior under these conditions. Thus in curve 2, a C-E minimum is clearly discernable at ca 0.05 V in both the positive- and negative-going voltammetric scans, reflecting the location of E_{pzc}. Similarly to the ac impedance data, a hysteresis in E_{min} obtained during positive- and negative-going potential sweeps is evident from some voltammetric data, such as curve 3 in Figure 2a. A significant additional feature of the voltammetric results, however, is the appearance of the sharp peak, labelled C_p in Figure 2a, centered at 0.57 V during positive-going

potential scans, but absent in negative-going sweeps. This characteristic feature, discussed in several earlier reports[1,2,16,17], is apparently associated with potential-induced removal of the surface reconstruction.

An interesting issue concerns the appearance of C_p upon altering the positive as well as negative limit of the cyclic voltammetric potential scans. Consistent with the foregoing assertions, C_p is only discernable if the lower potential limit is below 0.1 V (in 1 mM $HClO_4$), and increases as this limit is made more negative and if the potential is held at such negative values (vide infra). More unexpected, however, is the behavior seen by varying the upper potential scan limit. If the limit is set at potentials *just* positive of C_p dotted curve 1), this peak is observed clearly on the subsequent positive-going scan (Figure 2a). Setting the upper limit at higher potentials, 0.7 to 0.8 V, just below the onset of anodic oxide formation (dashed curve 2), however, leads to an *absence* of C_p on the subsequent positive-going sweep even when the lower potential limit is chosen to be at substantial negative values, such as -0.5 V. On the other hand, selecting the upper potential limit at sufficiently more positive values so that oxide formation and removal occurs yields again a clearcut reappearance of C_p during the subsequent positive-going scan (solid trace, Figure 2a). Consequently, then, altering the upper potential limit appears to influence the kinetics of reconstruction occurring during the next voltammetric cycle, and in a non-monotonic fashion. Comparable behavior has also been observed in sulfuric acid electrolyte (Figure 7a, b in ref. 16).

So far, we have presented results which concern the double-layer consequences of Au(100) reconstruction during repeated potential cycles. Of particular interest, nevertheless, is the effect upon the double-layer structure of the extensive reconstruction seen by STM to occur in perchloric acid electrolytes upon holding the potential at values negative of ca -0.2 V[5,6].

To this end, Figure 3a shows C-E curves obtained by ac impedance (20 Hz) during positive-going potential sweeps at 5 mV s^{-1} following various holding times (t_h = 0, 5, 10 min, as indicated) at -0.4 V in 1 mM $HClO_4$. Increasing the time spent at -0.4 V is seen to yield marked alterations in the shape of the C-E curves obtained during the subsequent positive-going potential scans (cf Figure 1). Thus for t_h = 10 min, the C-E well is substantially broader than for t_h = 0 min. Moreover, the former trace apparently features a *pair* of discernable, albeit shallow, C-E minima at about -0.03 and 0.10 V contained within the broad capacitance well (Figure 3a). Roughly comparable behavior was reported earlier in our preliminary communication, for Au(100) in 10 mM $HClO_4$[7]; the present data in 1 mM $HClO_4$ display clearcut C-E minima even for the longest t_h values.

The present results for Au(100) (Figure 3a) are compared alongside corresponding C-E data obtained for Au(210) in 1 mM $HClO_4$ in Figure 3b. The Au(210) surface was selected because it is known to exhibit negligible hysteresis in capacitance-potential behavior during potential cycles[18]. In contrast to Au(100), only minor changes in the shape of the C-E diffuse-layer minimum are seen for Au(210) upon increasing t_h at -0.4 V. One is therefore justified in asserting that the corresponding marked changes in the C-E morphology seen for Au(100) reflect the occurrence of surface reconstruction induced at negative charges.

Comparable changes are also observed in the C-E curves discerned from voltammograms obtained after holding the potential at such negative values. Representative voltammograms are shown in Figure 2b, obtained at 50 mV s^{-1} in 10 mM $HClO_4$. Similarly to Figure 2a, the solid trace shows a voltammetric cycle between -0.4 V and 1.3 V. Again, a small peak C_p is discernable at 0.57 V. The dashed trace, obtained by restricting the positive limit as for curve 2 in Figure 2a, also show an absence of peak C_p in the subsequent positive-going scan.

Holding the potential at -0.35 V for 20 min, however, yields a marked effect on the voltammogram. Besides a broadening of the C-E well and shifting to more positive potentials, as seen in the ac impedance data (Figure 3a), the peak C_p is seen to be enlarged substantially under these conditions

Some intriguingly direct information on the surface structural changes associated with the voltammetric feature C_p were obtained by acquiring STM data during such voltammetric sweeps. Figure 4a is an STM image acquired for Au(100) in 0.1 M $HClO_4$ during a voltammetric sweep at 10 mV s^{-1} after holding the potential at -0.4 V for 20 min. The image was obtained by scanning the tip from right to left as shown, and rastering upward. The scan speed is such that the acquisition of the entire image consumes about 20 s. The tip potential was held at 0 V. Since the electrode potential of the Au(100) surface is swept positive at 10 mV s^{-1} during the image acquisition, the y-axis can be considered to reflect linear variations of electrode potential as well as the microscopic distance scale shown. Thus the bottom and the top of the image correspond to electrode potentials of about 0.45 and 0.65 V, respectively. In the lower portion of the image, corresponding to potentials below 0.55 V, corrugated strands running diagonally are discernable. These strands are characteristic of the (5 × 27) reconstruction that is observed to form on Au(100) at negative charges[5,6]; the atomic details as observed by STM at higher resolution show that the strands propagate nearly parallel to the long dimension of the unit cell.*

---

*Strictly speaking, the reconstructed string directions can deviate by up to ca 20° from the substrate rows, commonly caused by the need for the reconstruction to circumnavigate step defects and the effects of terrace edges[6]. These differences in row angles can be accommodated in part by alterations in the directional propagation of the (5 × 27) unit cell, yet also by distortions in the unit-cell symmetry itself.

Interestingly, most of the corrugated strands in Figure 4a are seen to come to an abrupt end by the top quarter or so of the STM image, being replaced by arrays of gold "clusters" with typical x-y dimensions 2-3 nm. The previous images, taken at lower potentials, show the corrugated strands extending up to the top of the imaged area. Another example of an STM image taken under similar potential-sweep conditions (10 mV s^{-1}) is shown in Figure 4b. Again, the image was obtained by rastering upward, starting at 0.4 V vs SCE. This image illustrates how the reconstruction is lifted abruptly within a given domain, yet the potential at which this occurs is significantly (typically up to ca 50 mV) different between separate domains. Examination of "constant current" images as well as the "constant height" data** shown in Figure 4a indicates that the clusters are typically 1-3 atoms higher than the surrounding substrate. (The formation of small metal islands upon lifting the reconstruction on Pt(100), by CO adsorption in vacuum, has also been observed by STM[19].) Most significantly, the potential at which the reconstruction is seen to be lifted abruptly, 0.55-0.6 V, coincides with the position of the C_p peak measured independently under the same conditions in 0.1 M $HClO_4$. These data therefore provide irrefutable evidence supporting the earlier deduction of Schneider and Kolb that C_p arises from lifting sharply the Au(100) reconstruction, yielding localized deposits of excess gold atoms[2]. (Indeed, such peaks are commonly observed on Au(100) in other, more strongly adsorbing, electrolytes[1]). They arise physically from the

---

** Note that using the "constant height" (i.e. variable tunneling current) mode, protrusions such as the gold clusters appear brighter (higher current) on the right-hand side, since the tip (scanning from right to left) does not immediately undergo a z-displacement upon encountering the surface undulations. The left-hand side of the clusters appear darker since the tunneling current diminishes once the tip height becomes adjusted.

need to charge the electrode to more positive values so to compensate for the differences in the capacitive and E_{pzc} properties of the (5 × 27) and (1 × 1) surfaces.

It is noteworthy, however, that the extensive presence of small gold clusters upon sweeping the potential above C_p in perchloric acid shows that uniform (1 × 1) surface domains are not formed initially under these conditions. Nevertheless, STM images taken later in the voltammetric cycle, especially at potentials into the oxide region, above ca 1.0 V, and during the subsequent negative-going sweep show a significant and ultimately substantial aggregation of the gold clusters into larger (1 × 1) terraces. Reformation of the reconstruction is seen to be initiated as the potential is swept below about 0 V. We will discuss in detail elsewhere such coupled voltammetric - STM data; among other things, these demonstrate an interesting dependence of the ensuing surface morphology as well as the dynamics of surface reconstruction and its removal upon the adsorbing properties of the electrolyte anion[20].

It is appropriate to note that some aspects of the phenomena discussed here are dependent upon the details of the annealing procedure used to pretreat the Au(100) surface. Thus cooling the crystal at least partly in argon (or air) prior to immersing in water yields extensive reconstructed domains as observed by STM either in air[7] or after transferring to 0.1 M $HClO_4$ and held at ca 0.1 to 0.3 V. However, for freshly annealed crystals cooled to a greater extent in water, as in the case here and in earlier reports from CNRS (e.g. refs. 1,7,16), predominantly (1 × 1) (i.e. unreconstructed) surface domains are observed initially by in-situ STM under these conditions[7]. This initial marked difference in the surface atomic structure of Au(100) is also reflected in the cyclic voltammetry. Most notably, fresh surfaces displaying predominantly reconstructed domains to STM yield more pronounced peaks, similar to C_p, at about

0.6 V vs SCE in $HClO_4$, that are again associated with the sharp potential-induced removal of the reconstruction. (Indeed, Figure 4B is an example of this phenomenon for such *thermally*, rather than electrochemically, produced reconstruction.) Such variations in the annealing-cooling procedure can also account for some observed differences in the initial voltammetric behavior of Au(100) as reported by Kolb et al[2] and by Hamelin[1,7]. This issue will be addressed more fully elsewhere[20].

Implications for Double-Layer Heterogeneity

In order to interpret structurally the broadening of the C-E well observed upon Au(100) reconstruction, it is instructive to examine the morphology of the C-E minimum for the *unreconstructed* surface in comparison with the diffuse-layer predictions. The dashed trace in Figure 1b is a capacitance-charge density (C-σ) curve extracted from the corresponding dashed C-E curve given in Figure 1a, which as noted above refers essentially to an unreconstructed Au(100) surface in 1 mM $HClO_4$. The solid C-σ trace in Figure 1b was extracted from the corresponding inner-layer capacitance-charge density (C_{in}-σ) curve, obtained from C-E data in concentrated perchloric acid (as given in ref. 15), along with calculated diffuse-layer capacitances, C_{diff}, as a function of σ as obtained from Gouy-Chapman theory by using the usual formula

$$C_{calc}^{-1} = C_{in}^{-1} + C_{diff}^{-1} \qquad (1)$$

The conversion from C-E to C-σ data was accomplished by integration assuming that $E_{min} = E_{pzc}$ (i.e., where $\sigma = 0$).

The experimental and calculated C-E curves obtained in this manner (Figure 1b) are seen to be in reasonable concordance, especially in view of the assumptions necessarily involved. Most significantly in the present context, the

"breadth" of the C_{calc} – σ curve matches reasonably with the experimental trace, even though the minimum C_{calc} value ($7\mu F\ cm^{-2}$) is significantly lower than that observed. (The latter discrepancy probably arises in part from the occurrence of slight perchlorate specific adsorption at E_{pzc}[15,21].) Comparable findings were obtained from the same analysis applied to the corresponding C–E data for Au(210) in 1 mM $HClO_4$, except that the fit between the experimental and calculated C–σ curves is significantly better in this case.

Consequently, then, the observation of substantially broadened C–E wells in the vicinity of E_{pzc} upon partial or extensive reconstruction of Au(100), produced by excursions to negative electrode charges, indicates that a breakdown in the simple uniform-charge model embodied in the above double-layer analysis is being encountered under these conditions. Rather, the diffuse layer senses a distribution of local charge densities within the inner layer, so that while the average charge approaches zero at E_{min}, in actuality there is a range of differing E_{pzc} values, each associated with a given microscopic inner-layer structure. It is well known that E_{pzc} for gold is sensitive to the crystallographic orientation, decreasing markedly (by up to 0.35 V) in passing from the hexagonal close-packed Au(111) surface to other faces, such as Au(110), which feature more "open" structures as characterized, for example, by the average surface coordination number[17]. The simultaneous presence of local surface structures on reconstructed Au(100) which mimic electrostatically such varying behavior can therefore account qualitatively for the observed breadth of the C–E minimum induced by surface reconstruction. As discussed previously [14,22], however, the detailed nature of the C–E and (C–σ) response will depend upon the average dimensions of the electrostatically distinct inner-layer "patches", d_{ip}, in relation to the diffuse-layer thickness as gauged by the Debye length, κ_D. The diffuse layer will sense an apparently uniform inner layer only

when $d_{in} << \kappa_D$. When either (a) $d_{in} \sim \kappa_D$, or (b) $d_{in} >> \kappa_D$, the effects of inner-layer nonuniformity should prevail. In case (b), one expects that each inner-layer region will provide an independent contribution to the next C-E response, whereas for case (a) these components will tend to merge increasingly as d_{in} decreases relative to κ_D.

In practice, the distinction between case (a) and (b) is not straightforward, especially when there are several distinct inner-layer domains whose E_{pzc} values do not differ greatly, so that separate C-E minima may not occur even for case (b). Nevertheless, the observation of a broadened C-E well and the suggested resolution of a pair of minima upon charge-induced reconstruction (Figure 3a) is indicative that inner-layer nonuniformities are present having domain sizes at least comparable to κ_D.

This raises the interesting issue of the physical nature of these electrostatically distinct domains. As clearly seen from STM images obtained for electrochemically reconstructed Au(100) at various magnifications[6], the reconstructed Au(100) regions commonly consist of long ($\geq$ 50 nm) "strands" propagated close to the long direction of the unit cell. The domain size *across* such strings nevertheless tends to be rather smaller, typically of the order of 10–20 nm or less, patches of (1 × 1) substrate surviving in between adjacent strands. These latter dimensions are comparable to the Debye length for the 1 mM electrolyte employed in Figures 1a and 3a, $\kappa_D \sim 9.5$ nm. Although the local E_{pzc} of the reconstructed Au(100) regions is somewhat uncertain, one can surmise that the quasihexagonal atomic packing will yield more positive E_{pzc} values, closer to that for Au(111). This notion is in harmony with the observed 0.15–0.25 eV higher work function for reconstructed compared with unreconstructed Au(100) in ultrahigh vacuum[23].

Given their dimensions, along with the observed survival of adjacent (1 ×

1) patches, the formation of such reconstructed domains can account on the basis of either case (a) and (b) above for the broadening and shifting of the C-E well towards slightly higher potentials under these conditions. (These changes can be discerned by comparing the C-E curves obtained during positive- rather than negative-going sweeps in Figure 1a, as well as after holding at -0.35 V in Figure 3a). However, it is important to note that the presence of significant surface components having local E_{pzc} values *lower* as well as higher than for the unreconstructed surface is implicated by the broadening of the C-E well also towards more negative potentials under these conditions (Figure 3a). This finding can again be rationalized by referring to the STM images in ref. 6. The presence of domain edges between the (5 × 27) and (1 × 1) domains is seen to abound under these conditions. In addition, the longwise propagation of the reconstructed domains commonly involves "jogs" so that the strands circumnavigate ("bend around") surface defects. These factors produce an array of gold atomic corrugations not unlike those characteristic of Au(110) and higher-index faces[8,9,13]. It is well known that such corrugated surfaces exhibit E_{pzc} values that are 0.1-0.2 V below that for unreconstructed Au(100)[17,24]. Consequently, the presence of atomic corrugation associated in particular with the edges of reconstructed strands, along with surface defects, can yield inner-layer nonuniformities having dimensions, d_{in}, that satisfy case (a) or (b) above, and thereby can broaden the overall C-E well towards lower potentials.

A related illustration of the effects of inner-layer nonuniformity on the C-E profile is provided in Figure 5. Here, C-E curves in 11 mM KPF_6 for Au(111), (100), and (110) (dotted, dashed-dotted, dashed traces, respectively) are shown, obtained during 5 mV s^{-1} positive-going potential sweeps from -0.6 V. A corresponding C-E curve obtained for a polycrystalline gold surface, polished and annealed in the same way as the single-crystal faces, is given for comparison.

The C-E well for the polycrystalline surface is seen to be considerably broader and asymmetric, and apparently contains components from the three low-index faces. This finding is consistent with the expectations of case (b) above, and therefore suggests that "monocrystalline facets" with dimensions larger than the Debye length under these conditions, $\kappa_D \approx 3$ nm, are present on the annealed polycrystalline surface.

Electrochemical Kinetics

The foregoing results demonstrate that the occurrence of electrochemically induced reconstruction of Au(100), while yielding large surface domains with hexagonal surface packing reminiscent of Au(111), yields a net double-layer behavior more consistent with the presence of a mixture of structures, including elements of "higher-index" faces. Given the observed sensitivity of the rates of proton electroreduction to the gold surface crystallographic orientation[10,11], it is of some interest to examine the kinetic behavior of the "composite" reconstructed, compared with the (1 × 1), Au(100) surface.

The procedures employed to obtain faradaic currents, i_f, for proton electroreduction, and hence rate constants k_{ob} (cm s^{-1}), as a function of the electrode potential E were primarily as outlined in ref. 10. After annealing, a cyclic voltammogram was recorded to check the surface state. The electrolyte used was 0.09 M $NaClO_4$ + 0.01 M $HClO_4$. The i_f - E data were extracted by sweeping the potential negative, up to about -0.7 V, at 5 mV s^{-1}. The possible distorting effect of uncompensated solution resistance upon the i_f - E data was not considered earlier[10,11]. To check this effect, i_f - E data were obtained for Au(210) successively in the presence and absence of positive-feedback iR compensation under otherwise identical conditions (cf ref. 25). The Au(210) surface was chosen for this purpose in view of its extremely reproducible kinetic

behavior (including the absence of any hysteresis in the i_f - E curves obtained for negative- and positive-going potential sweeps)[10,11]. Figure 6 shows resulting log k_{ob} - E plots obtained in this fashion, for Au(210) in 0.09 M $NaClO_4$ + 0.01 M $HClO_4$, in the presence (circles) and absence (triangles) of iR compensation. The distorting influence of the electrolyte iR drop is seen to be significant only at higher overpotentials. While removing this artifact necessarily diminishes the curvature in the log k_{ob} - E plot, the corrected version still exhibits noticeable nonlinearity. The remaining kinetic data reported here were obtained with appropriate iR compensation.

In order to ascertain the effects of Au(100) reconstruction upon the proton electroreduction rates on this surface, it is clearly necessary to compare i_f - E data obtained with and without prior holding at a suitably negative potential so to generate the reconstructed phase. Figure 7 shows a pair of log k_{ob} - E plots obtained for proton electroreduction in Au(100) with and without prior holding at -0.35 V for 6 min before sweeping at 5 mV s^{-1} to more negative potentials (open and filled circles, respectively). The rates on the reconstructed phase are seen to be about 1.3 to 1.7 fold higher at a given potential on the reconstructed surface. A complication with this procedure is that some reconstruction will inevitably occur at the negative potentials at which the proton electroreduction kinetics are evaluated even in the absence of prior potential holding. Most likely, then, the rate accelerations evident in Figure 7 are probably rather more modest than those actually arising from Au(100) surface reconstruction.

Another difficulty with this experimental procedure is that such differences in potential history may yield additional effects upon the ensuing i_f - E response, arising for example from the accumulation of surface impurities. This possibility was checked by acquiring i_f - E data on several other gold

faces, including Au(210), under the same conditions as the pair of Tafel plots shown for Au(100) in Figure 7. Most surfaces examined, even Au(210), yielded slightly (5–15%) higher i_f, and hence k_{ob}, values following prior potential holding at −0.35 V. (For Au(111), part of the small, ca 10%, rate increases may be connected with the mild ($\sqrt{3} \times 22$) reconstruction which is observed to develop at negative potentials over similar time periods (10–15 min) as for the Au(100) reconstruction[26,27].) Nonetheless, these differences were found persistently to be markedly smaller than those observed for Au(100). Consequently, then, we have some confidence in asserting that the observed ca 50% rate accelerations observed for Au(100) in Figure 7 arise predominantly from the alterations in substrate structure attending surface reconstruction.

A more cursory examination was also made into the effects of Au(100) surface reconstruction upon the electrooxidation of carbon monoxide in 0.1 M $HClO_4$. We have previously reported a detailed kinetic–infrared spectral study of this reaction, which exhibits a remarkably large sensitivity to the gold crystallographic orientation[12]. The rate–potential data were obtained essentially as described in ref. 12, employing anodic linear sweep voltammetry. For electrodes held at ca −0.3 V vs SCE for several minutes or more prior to obtaining the anodic voltammogram, so to yield primarily reconstructed Au(100), kinetic data for CO electrooxidation were obtained that are closely similar to those reported in ref. 12. Commencing the potential scan for a freshly annealed surface at higher values ($\gtrsim$ 0 V), so to electrooxidize CO on a largely unreconstructed surface, yielded voltammograms shifted to significantly (50–100 mV) higher overpotentials, indicative of slower kinetics. The latter conditions, however, yielded less reproducible voltammograms.

Implications of Electrode Kinetics

The occurrence of small yet significant rate accelerations for proton electroreduction upon Au(100) surface reconstruction can readily be interpreted on the basis of the double-layer behavior considered above. At first sight, one might anticipate that rate *decreases* would instead be observed. This expectation derives from our earlier observation that the proton electroreduction rates on Au(111) are about 1.3 to 2 fold smaller than ostensibly unreconstructed Au(100) under experimental conditions similar to those in Figure 6B[10]. Given that the Au(100) reconstructed domains consist of hexagonally packed gold atoms in a similar fashion to Au(111), together with the more generally observed correlation between the proton electroreduction rate and the surface coordination number of the gold atoms[10], comparably rates might be expected upon Au(100) reconstruction.

The observation of a *qualitatively* opposite effect indicates that other factors are at play here. The present double-layer analysis shows that the inner-layer structure is decidedly nonuniform, containing elements that are electrostatically more akin to stepped and other higher-index faces (vide infra). As already noted, our STM data for reconstructed Au(100) in ref. 6 shows the presence of numerous surface "jogs", domain edges, produced largely by segments of the enveloping (5 × 27) phase. It appears likely that such sites, featuring lower coordination numbers of the surface gold atoms, are responsible for the accelerated rates of proton electroreduction observed on reconstructed Au(100).

Physically, the enhanced reactivity may well arise from the anticipated stronger adsorption of the adsorbed hydrogen atom intermediate, produced by surface proton transfer, on gold sites having a lower coordination number (i.e. surrounded by fewer nearest-neighbor gold atoms). This explanation, indeed, can account for the observed correlation between log k_{ob} and E_{pzc} (and related

parameters) for a series of largely unreconstructed gold surfaces[10]. It is worth noting that the overall observed reaction rates on nonuniform surfaces, being the composite of an array of differing local rates, k_{loc}, will reflect predominantly the faster k_{ob} values. As a consequence, then, it is quite likely that the observed k_{ob} values for proton electroreduction on reconstructed Au(100) reflect chiefly the occurrence of reaction at "minority" sites, rather than on uniform terraces.

The observed moderate accelerating effect of Au(100) reconstruction upon the rates of CO electrooxidation can be interpreted along qualitatively similar lines. Thus the rate effects may arise in part from the stronger adsorption of CO on such lower-coordination number sites as detected by infrared spectroscopy[12]. However, other factors undoubtedly play a role, especially the coadsorption of water or hydroxyl groups on adjacent sites required for the oxygen-transfer reaction to take place[12].

Overall, the present findings show that the electrochemical kinetic as well as equilibrium double-layer properties of ordered Au(100) are affected significantly by surface reconstruction in a fashion which is more involved than that anticipated simply on the basis of the formation of hexagonal "Au(111)-like" terraces from the initial square-planar gold surface lattice. It clearly would be worthwhile to explore such phenomena for a range of initial surface states as induced by altering the annealing-cooling conditions, as well as in different, more adsorbing, electrolytes such as sulfuric acid[2]. The utilization of in-situ STM combined with voltammetry to explore further the structural and dynamical aspects of potential-induced reconstruction of Au(100), especially the role of adsorbing electrolyte anions, will be described elsewhere[20].

Acknowledgement

This work was supported in part by the U.S. Office of Naval Research.

REFERENCES

1. A. Hamelin, J. Electroanal. Chem., 142, (1982), 299.
2. J. Schneider and D.M. Kolb, Surf. Sci., 193, (1988), 579.
3. A. Friedrich, B. Pettinger, D.M. Kolb, G. Lüpke, R. Steinhoff, and G. Morowsky, Chem. Phys. Lett., 163, (1989), 123.
4. B.M.Ocko, J. Wang, A. Davenport, and H. Isaacs, Phys. Rev. Lett., 65, (1990), 1466.
5. X. Gao, A. Hamelin, and M.J. Weaver, Phys. Rev. Lett., 67, (1991), 618.
6. X. Gao, A. Hamelin, and M.J. Weaver, Phys. Rev. B, 46, (1992), 7096.
7. A. Hamelin, X. Gao, and M.J. Weaver, J. Electroanal. Chem., 328, (1992), 361.
8. X. Gao, A. Hamelin, and M.J. Weaver, Phys. Rev. B., 44, (1991), 10983.
9. X. Gao, A. Hamelin, and M.J. Weaver, Surf. Sci., 274, (1992), L588.
10. A. Hamelin and M.J. Weaver, J. Electroanal. Chem., 223, (1987), 171.
11. A. Hamelin, L. Stoicoviciu, S-C. Chang, and M.J. Weaver, J. Electroanal. Chem., 307, (1991), 183.
12. S-C. Chang, A. Hamelin, and M.J. Weaver, J. Phys. Chem, 95, (1991), 5560.
13. X. Gao, A. Hamelin, and M.J. Weaver, unpublished results.
14. M.A. Vorotyntsev, in "Modern Aspects of Electrochemistry", Vol. 17, J. O'M. Bockris, B.E. Conway, and R.E. White, eds, Plenum Press, New York, 1986, Chapter 2.
15. F. Silva, M.J. Sottomayor, A. Hamelin, and L. Stoicoviciu, J. Electroanal. Chem., 295, (1990), 301.
16. A. Hamelin, J. Electroanal. Chem., 255, (1988), 281.
17. A. Hamelin, in "Modern Aspects of Electrochemistry", Vol. 16, B.E. Conway, R.E. White, and J. O'M. Bockris, eds, Plenum Press, New York, 1985, Chapter 1.
18. A. Hamelin, Z. Borkowska, and J. Stafiej, J. Electroanal. Chem., 189, (1985), 85.
19. W. Hösler, E. Ritter, and R.J. Behm, Ber. Bunsenges. Phys. Chem., 90,

(1986), 205.

20. X. Gao, G. Edens, A. Hamelin, and M.J. Weaver, in preparation.

21. A. Hamelin and L. Stoicoviciu, J. Electroanal. Chem., 236, (1987), 267.

22. M.A. Vorotyntsev, J. Electroanal. Chem., 123, (1981), 379.

23. P.N. Ross and A.D. A'Agostino, Electrochim. Acta, 37, (1992), 615.

24. A. Hamelin and L. Stoicoviciu, J. Electroanal. Chem., 234, (1987), 93.

25. B.D. Cahan, H.M. Villulas, and E.B. Yeager, to be published.

26. X. Gao, A. Hamelin, and M.J. Weaver, J. Chem. Phys., 95, (1991), 6993.

27. N.J. Tao and S.M. Lindsay, Surf. Sci., 274, (1992), L546.

Figure Captions

Figure 1

a) Differential capacitance-electrode (C-E) curves obtained for Au(100) in 30 and 1 mM $HClO_4$, as indicated, during potential cycling at 5 mV s^{-1} between -0.5 and 1.35 V in the directions indicated. (Dotted trace for 30 mM $HClO_4$ refers to positive-going sweep from -0.1 V.)

b) Capacitance-electrode charge density (C-σ) curve for unreconstructed Au(100) in 1 mM $HClO_4$ (dotted trace), extracted from C-E curve obtained during negative-going potential scan in (a). Corresponding solid trace was calculated from the Gouy-Chapman model by using Eq. (1), along with inner layer capacitance - σ data extracted from Fig. 6 of ref. 15.

Figure 2

a) Cyclic voltammograms obtained at 50 mV s^{-1} for Au(100) in 1 mM $HClO_4$ for various positive potential limits.

b) Cyclic voltammograms obtained at 50 mV s^{-1} for Au(100) in 10 mM $HClO_4$, showing the effect of forming the surface reconstruction by holding at -0.35 V (see text for details).

Figure 3

a) Differential capacitance-potential (C-E) curves obtained for Au(100) in 1 mM $HClO_4$ during positive-going sweep following holding at -0.4 V for times t_h(min), as indicated.

b) As for (a), but for Au(210) [insert shows ball model for the (210) surface].

Figure 4

In-situ STM images of Au(100) in 0.1 M $HClO_4$, obtained during 10 mV s^{-1} positive-going voltammetric sweeps, showing potential-induced removal of surface reconstruction. Images obtained by rastering the tip upwards, so that substrate electrode potential is about 0.45 V at the bottom, and 0.65 V by the top of the image. Reconstruction in (a) formed by prior potential holding at -0.4 V for 20 min; in (b) by prior surface annealing followed by cooling partly in nitrogen.

Figure 5

Differential capacitance-potential (C-E) curves obtained in 11 mM KPF_6 for Au(111) (dotted), Au(100) (dashed-dotted), and Au(110) (dashed trace), obtained during 5 mV s^{-1} positive-going sweep from -0.6 V. Solid trac corresponding curve for a polycrystalline surface prepared (polished, annealed) in the same fashion.

Figure 6

Logarithm of observed rate constant for proton electroreduction versus electrode potential for Au(210) in 0.090 M $NaClO_4$ + 0.01 M $HClO_4$, in the presence (circles) and absence (triangles) of iR compensation.

Figure 7

Logarithm of observed rate constant for proton electroreduction versus electrode potential on largely unreconstructed (filled circles) and reconstructed Au(100) (open circles) in 0.09 M $NaClO_4$ + 0.01 M $HClO_4$ (see text).

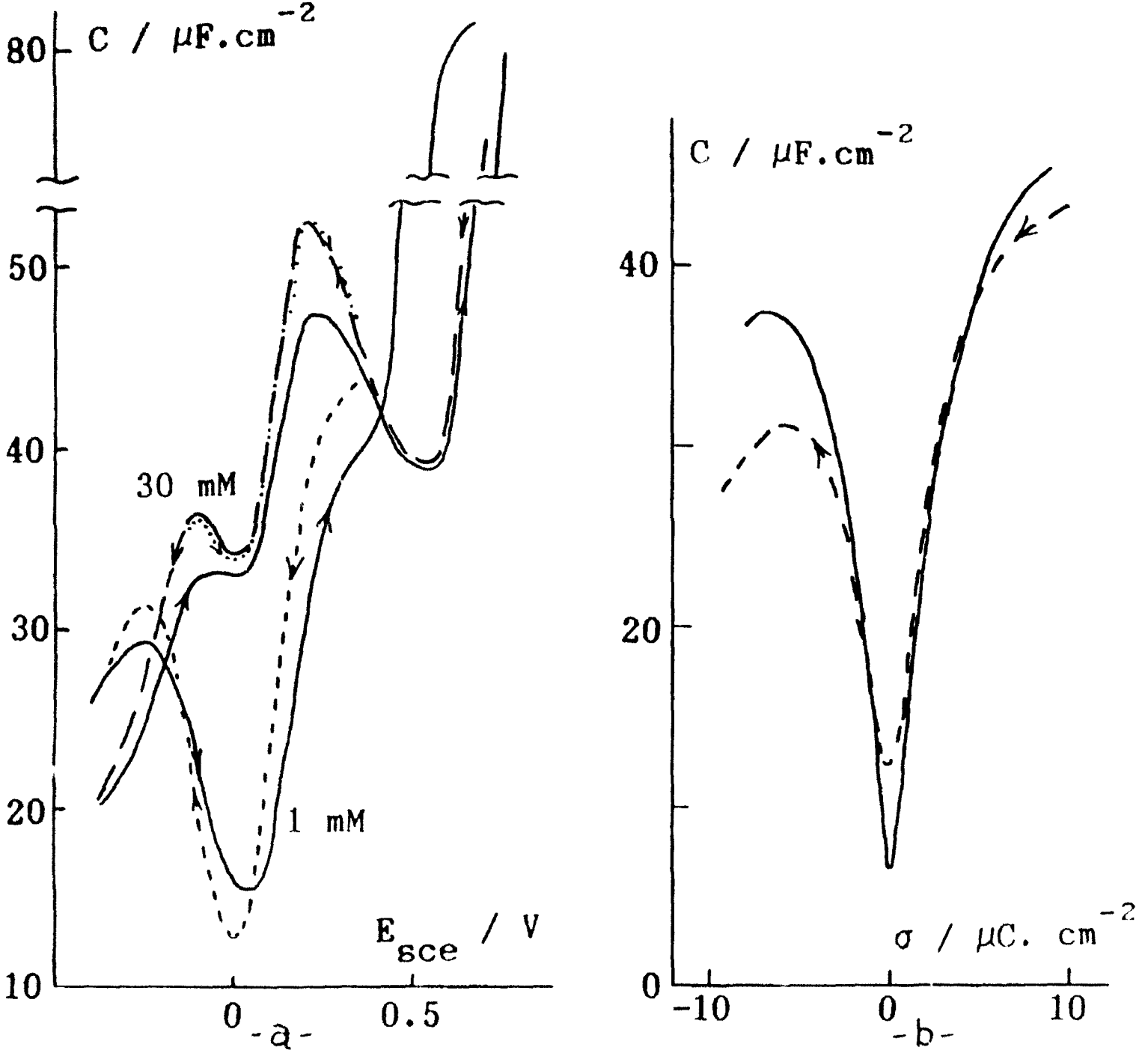
C / μF.cm⁻²
80
50
40
30
20
10
30 mM
1 mM
E sce / V
0
0.5
-a-
C / μF.cm⁻²
40
20
0
σ / μC. cm⁻²
-10
0
10
-b-

Fig. 2

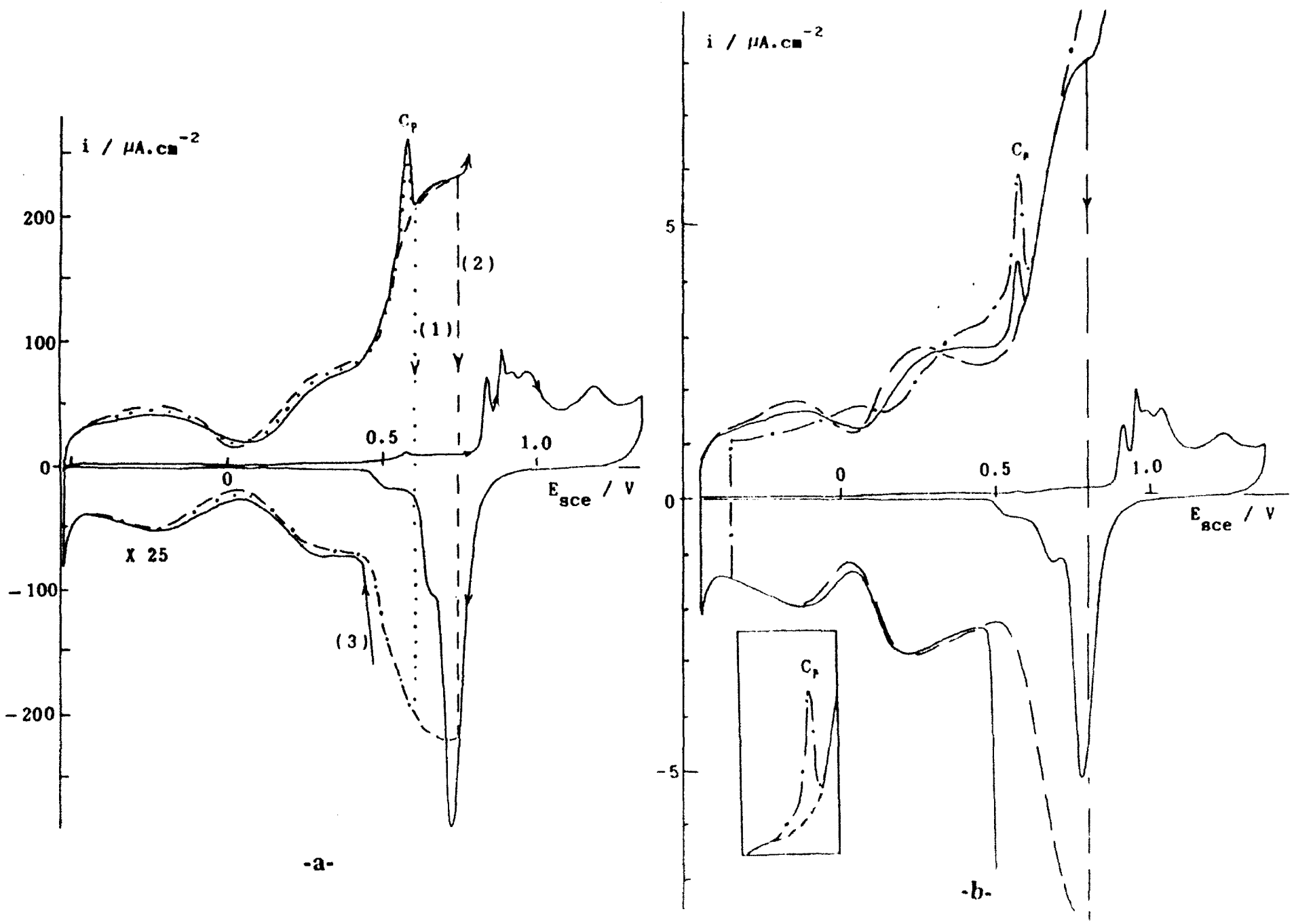
i / μA.cm⁻²
200
100
0
-100
-200
Cp
(1)
(2)
(3)
0.5
1.0
0
X 25
Esce / V
-a-
i / μA.cm⁻²
5
0
-5
Cp
0
0.5
1.0
Esce / V
-b-

Fig.2

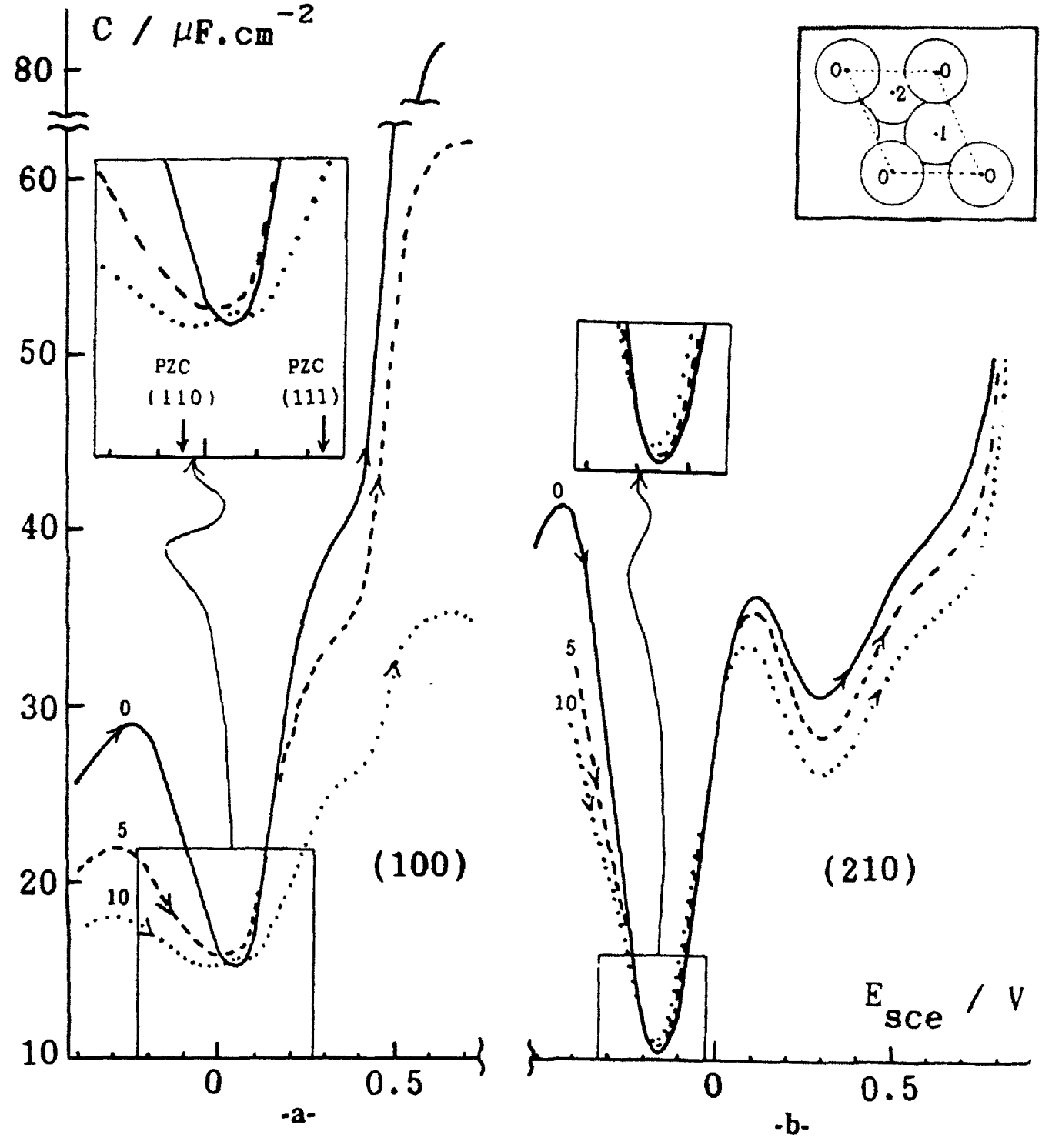
C / μF.cm⁻²
80
60
50
40
30
20
10
PZC
(110)
PZC
(111)
0
5
10
(100)
0
0.5
-a-
0
5
10
(210)
E sce / V
0
0.5
-b-
0
0
-2
-1
0
0

Fig. 3

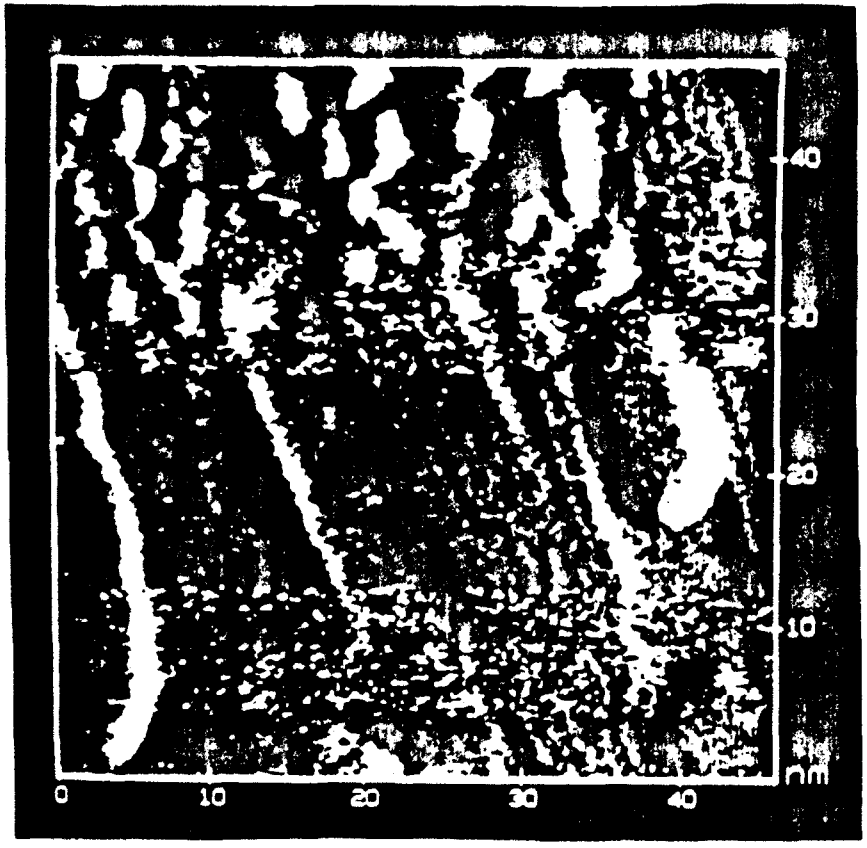

A

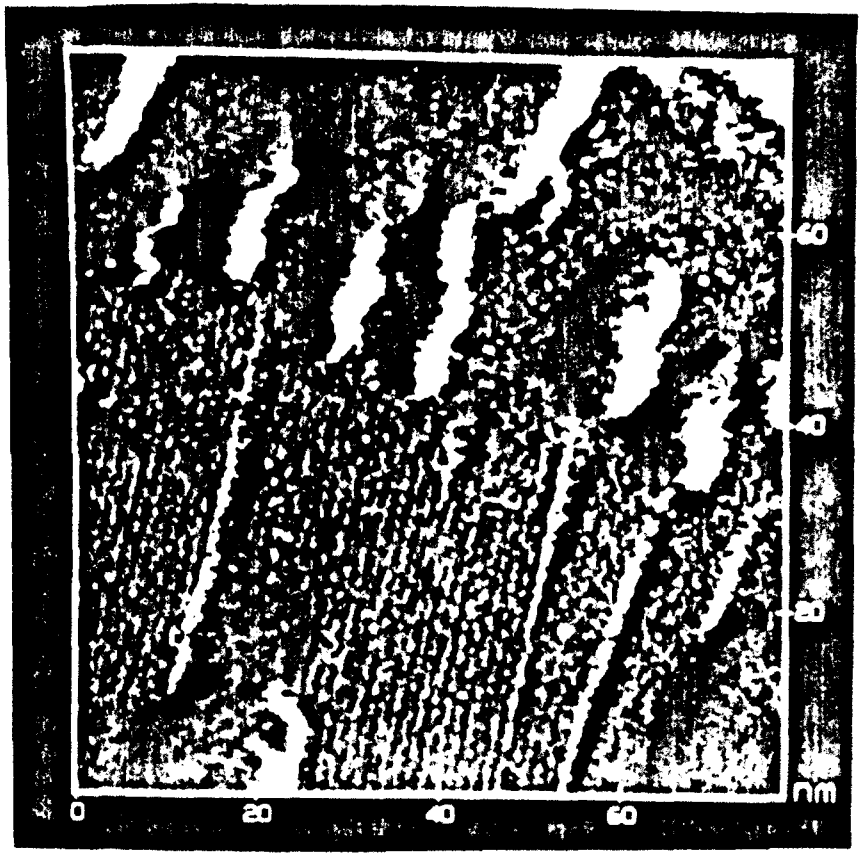

B

FIG 4

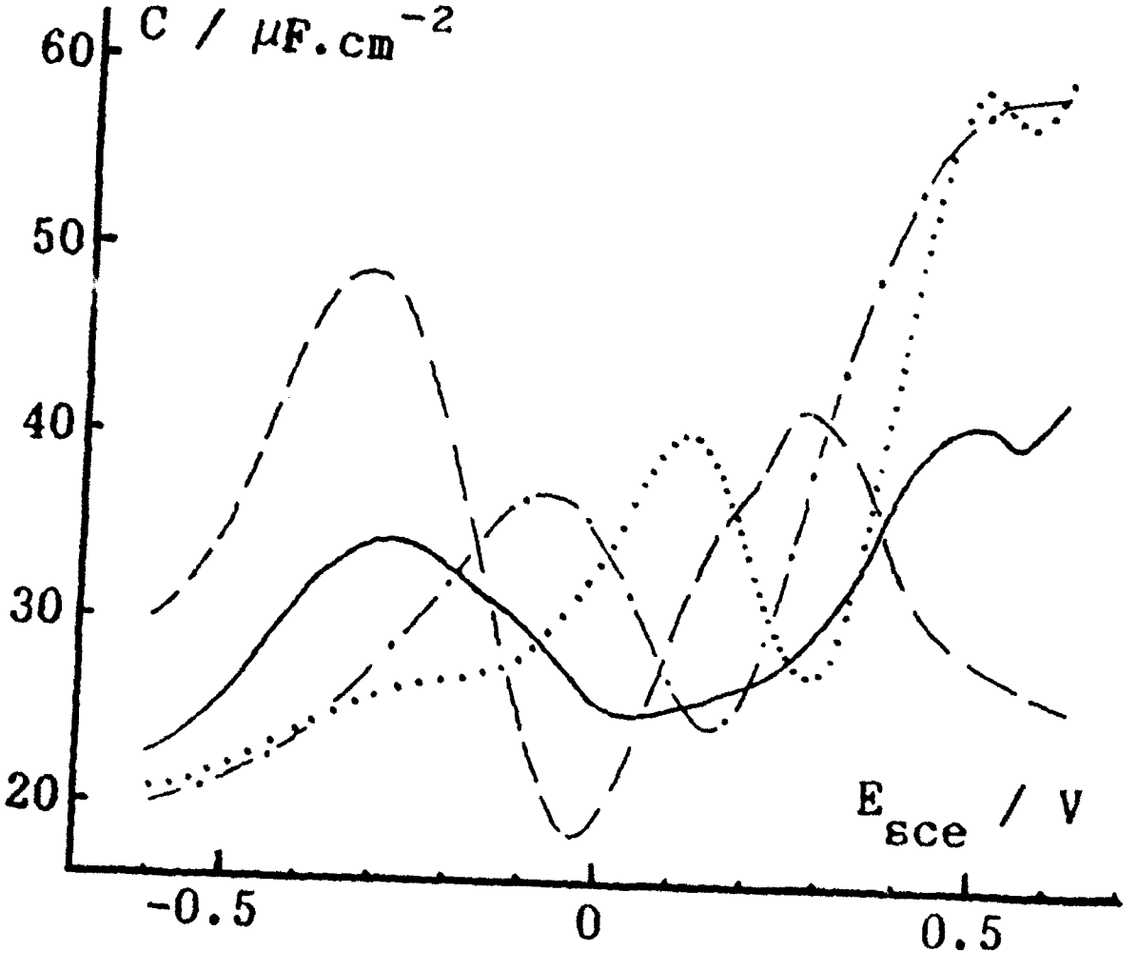

Fig. 5

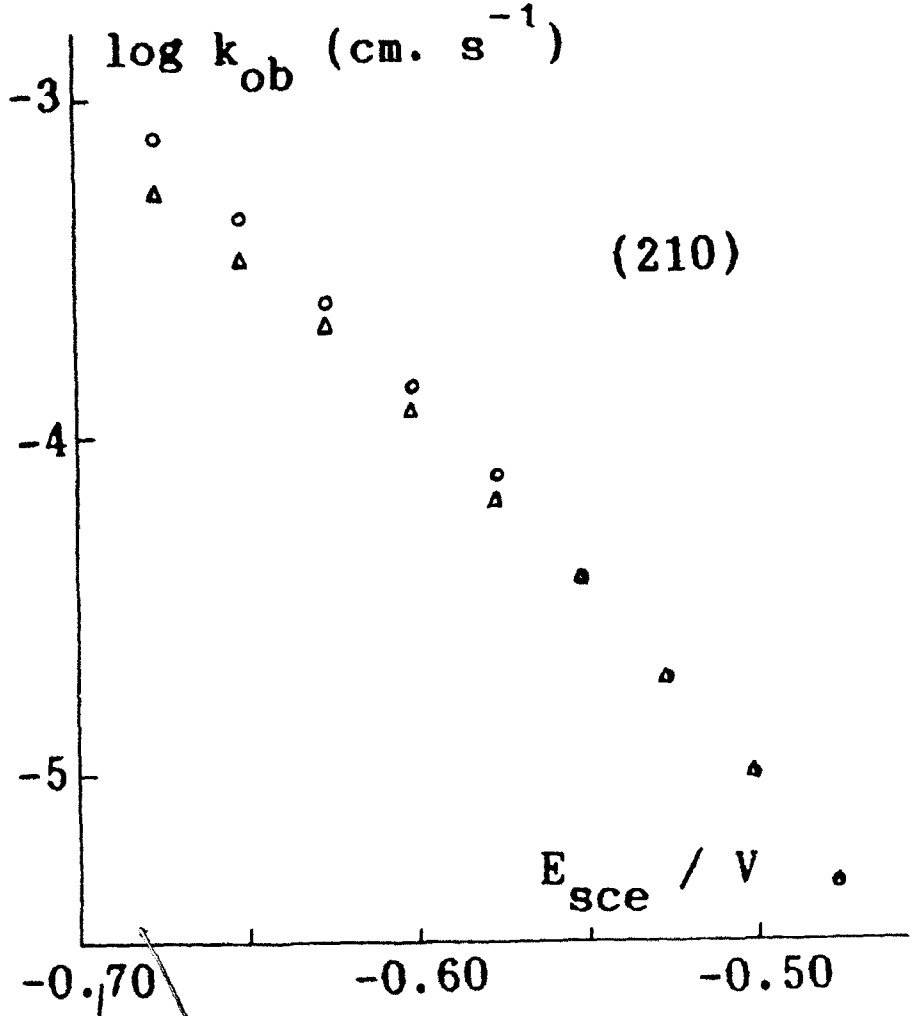

Fig.6

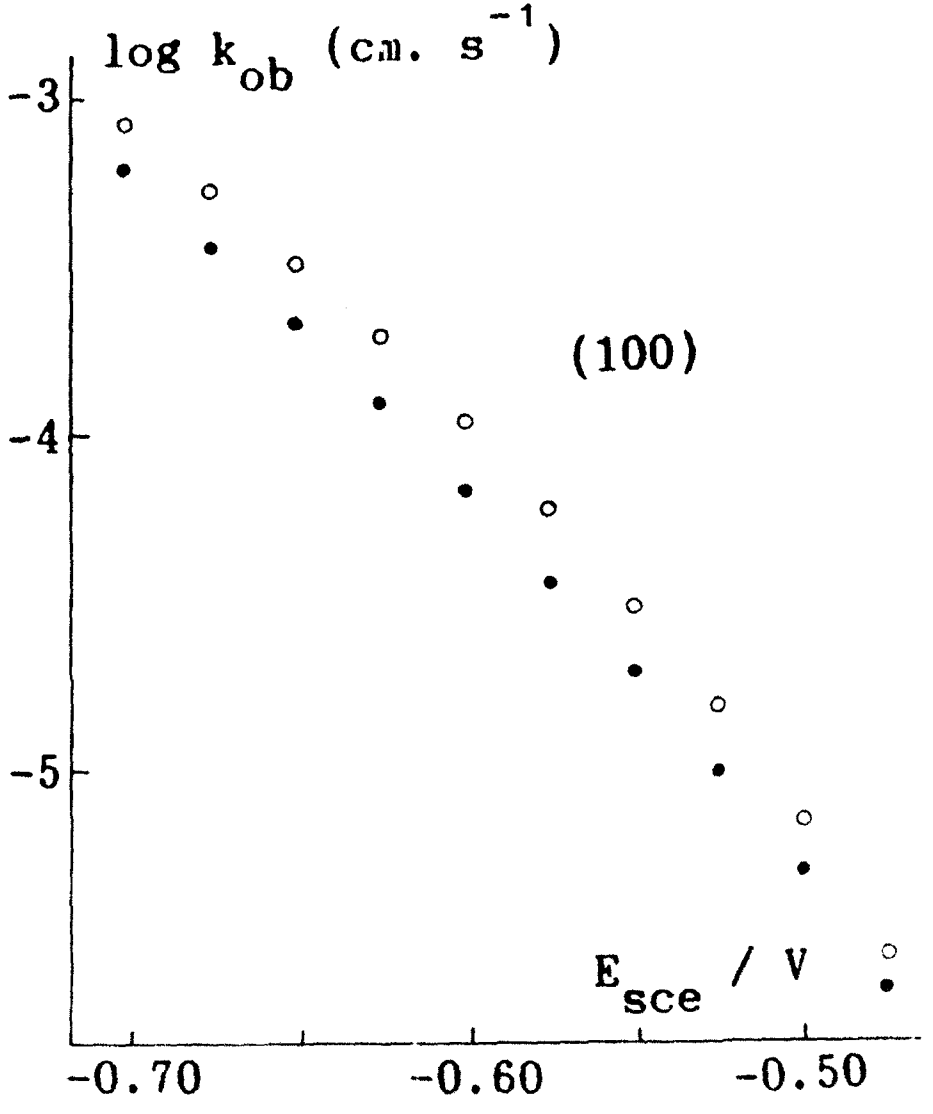

Fig. 7

to be published side by side